

Imaging with the CHARA interferometer

Ettore Pedretti^{a,*}, John D. Monnier^b, Theo ten Brummelaar^c, Nathalie D. Thureau^a

^a*School of Physics and Astronomy, University of St Andrews, North Haugh, St Andrews KY16 9SS, Scotland.*

^b*University of Michigan, Astronomy dept., 914 Dennison bldg., 500 Church street, Ann Arbor, MI, 40109, USA*

^c*Center for High Angular Resolution Astronomy, Georgia State University, P.O. Box 3969, Atlanta, GA 30302-3969, USA*

Abstract

The very long baseline interferometer (VLBI) can achieve the highest angular resolution imaging of any telescope at radio wavelengths using thousand-kilometre baselines. The deployment at the center for high angular resolution astronomy (CHARA) array of new beam combiners has enabled the imaging capabilities of the array. CHARA can now obtain images with an angular resolution similar to the VLBI but using hundred-metre baselines. This is achieved by operating the array at the shorter wavelengths of optical and infrared light. We review the successful deployment of the Michigan infrared combiner at the CHARA array and discuss some of the imaging results from this instrument.

Key words:

Technique: interferometric; Methods: data analysis; Instrumentation: interferometers

1. Introduction

First generation optical interferometers (Labeyrie, 1975; Labeyrie et al., 1986; Shao et al., 1988; Dyck et al., 1995) obtained interference fringes by coherently combining the light of two separate telescopes. The fringes contained both amplitude and phase information but only the amplitude was usable. The measured phase was corrupted by the random modulation from the atmosphere. Two-telescope interferometers were capable of model-dependent imaging. For example, star diameters could be measured by fitting a simple one-parameter “uniform disc” model to the observed visibilities.

The first image ever produced by an optical interferometer using separate telescopes was the binary star Capella (Baldwin et al., 1996), that was obtained at the Cambridge optical aperture synthesis telescope (COAST). When more than two telescopes are used a quantity called “closure phase” can be measured (Jennison, 1958). The closure phase is the sum of three fringe phases around a closed triangle of baselines. See Monnier (2007) for an introduction to closure phase measurement.

Closure phases are more robust to calibration error than visibility amplitudes. Atmospheric turbulence generally does not bias their measurement and there is a reasonable expectation of the measurement error reducing as \sqrt{N} , where N is the number of measurements (Buscher, 1988).

Closure phases are sensitive to asymmetries in the brightness distribution. Only centro-symmetry yields closure phase of 0° or 180° . Image reconstruction software developed for radio interferometry can be modified to use visibilities and closure-

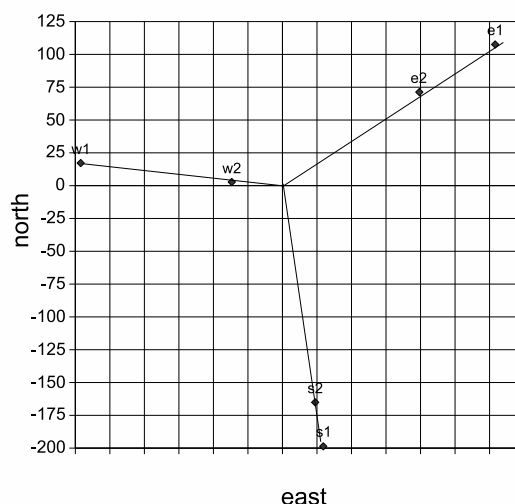


Figure 1: The positions and orientations of the CHARA telescopes at Mount Wilson. The coordinates are in metres and the origin is the centre of the array.

phases, allowing model-independent imaging for optical interferometers.

1.1. The CHARA array

The Center for High Angular Resolution Astronomy at Georgia State University aims to apply high angular resolution techniques to the study of astronomical objects. For this purpose CHARA built an interferometric array on Mount Wilson, California (ten Brummelaar et al., 2005). The array is composed of six one-metre telescopes on a Y-shaped configuration. Figure 1 shows the position of the telescopes with respect to the centre of the array.

*Corresponding author

Email addresses: ep41@st-and.ac.uk (Ettore Pedretti)

¹Scottish Universities Physics Alliance (SUPA)

Table 1: The angular resolution of well-known observatories compared to the CHARA array.

Observatory	Wavelength λ (μm)	Baseline (m)	Angular resolution (milli-arcseconds)
Hubble Space Telescope	0.5	2.4	43.0
Keck Telescope	1.65	10.0	34.0
CHARA Array	0.5	330.0	0.3
Very Long Baseline Array	10^4	8.6×10^6	0.24

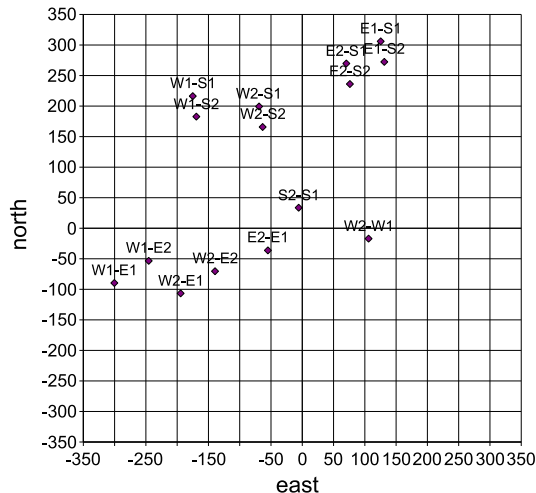


Figure 2: The length and orientation of the CHARA baseline vectors at glance.

The baselines of the array are non-redundant. CHARA can deliver 15 visibility amplitude and 10 independent closure-phase triangles when all six telescopes are combined together. The maximum baseline length of the array is 330 m. The corresponding angular resolution is 0.3 to 1 milli-arcsecond from visible to near-infrared respectively. The length and orientation of the baselines are shown in Figure 2 and are also reported on Table 2 (ten Brummelaar et al., 2005).

It is of interest to compare the angular resolution of the CHARA array with other observatories. Table 1 lists the wavelength of operation, baseline and angular resolution of several observatories. At visible wavelength the angular resolution of CHARA is directly comparable to the Very Long Baseline interferometer. In the future this will permit a direct comparison of the optical and radio image of the same source.

The CHARA array has already produced unique science in the two-telescope and four telescope configuration. Notably it has provided calibration of the Baade-Wesselink relation by directly measuring the ‘‘P-factor’’ (Mérand et al., 2005), the first detection of gravitational darkening in a rapidly-rotating star (McAlister et al., 2005; van Belle et al., 2006), measurement of the diameter of an exoplanet using transit and interferometric diameter of the host star (Baines et al., 2007), the first image of a main sequence star (Monnier et al., 2007) and the first image of an interacting binary (Zhao et al., 2008a)

1.2. Beam combiners at CHARA

Several beam combiners have been deployed at the CHARA interferometer in the last few years. The performances of these combiners are listed on table 3. Historically the first beam combiner available at CHARA was CHARA Classic, a simple bulk-optics, pupil-plane combiner capable of combining two telescope at times, operating from 1.5 to 2.5 μm . This instrument is not an imaging combiner since combining only two telescopes does not produce closure phase. The first science results from the CHARA array were obtained with the CHARA Classic instrument and with the fiber linked unit for recombination (FLUOR) instrument (McAlister et al., 2005; van Belle et al., 2006; Bagnuolo et al., 2006; Berger et al., 2006a; Aufdenberg et al., 2006)

FLUOR is a two-telescope combiner that measures visibilities with 1% precision, therefore allows high accuracy stellar diameter measurement (Coudé du Foresto and Ridgway, 1992; Coudé du Foresto et al., 1997). The instrument was first tested on the solar telescope at Kitt Peak in Arizona and then deployed at the infrared optical telescope array (IOTA). In 2001 it was transferred at the CHARA interferometer (Coude du Foresto et al., 2003). FLUOR is also a non-imaging combiner since it allows only a two-telescope combination.

Access to visible wavelengths is now granted to CHARA through two new beam combiners, the visible spectrograph and

Table 2: The baselines of CHARA (ten Brummelaar et al., 2005).

Telescope designation	East (m)	North (m)	Height (m)	Baseline (m)
S2-S1	-5.75	33.58	0.64	34.08
E2-E1	-54.97	-36.25	3.08	65.92
W2-W1	105.99	-16.98	11.27	107.93
W2-E2	-139.48	-70.37	3.24	156.26
W2-S2	-63.33	165.76	-0.19	177.45
W2-S1	-69.08	199.35	0.45	210.98
W2-E1	-194.45	-106.62	6.32	221.85
E2-S2	76.15	236.14	3.43	248.13
W1-S2	-169.32	182.74	-11.46	249.39
W1-E2	-245.47	-53.39	-8.03	251.34
W1-S1	-175.07	216.32	-10.82	278.5
E2-S1	70.4	269.72	-2.79	278.77
E1-S2	131.12	272.38	-6.51	302.37
W1-E1	-300.44	-89.64	-4.95	313.57
E1-S1	125.37	305.96	-5.87	330.71

Table 3: Performance of beam combiners at CHARA.

Instrument	Faintest magnitude reached	Wavelength λ (μm)	R ($\lambda/\Delta\lambda$)	Visibility accuracy	Closure-phase accuracy ($^\circ$)
CHARA Classic	7.5	1.50 – 2.50	NA	5 – 10% typical	NA
FLUOR	6.0	2.20	NA	1% typical	NA
MIRC	4.5	1.50 – 2.40	40, 150, 400	10% or worse	0.1 – 0.5
VEGA	7.4	0.45 – 0.90	30000, 5000, 1700	3%	??
PAVO	8.2	0.66 – 0.95	40	2%	??

polarimeter (VEGA) and the precision astronomical visible observations (PAVO). VEGA was originally in use at the grand interféromètre à deux télescopes (GI2T) (Mourard et al., 1994) and was recently rebuilt and updated for the CHARA array (Mourard et al., 2008). Its wavelength of operation is from 0.45 to 0.9 μm . VEGA is coupled to the spectro-polarimetric interferometry (SPIN) instrument (Chesneau et al., 2000) to study stellar polarization phenomena. VEGA employs two Algol “comptage de photon nouvelle génération” (CPNG) detectors (Blazit et al., 2008). The spectral resolution in dispersed fringes mode is $R=1500$ with one camera, $R=6000$ and $R=30000$ with two cameras. VEGA has imaging capabilities in the visible since it has successfully combined three beams and will eventually allow four beam combination in the near future.

PAVO is also a visible beam combiner for the CHARA array optimized for sensitivity (Ireland et al., 2008). PAVO has already reached one magnitude fainter than the VEGA instrument due to its high quantum efficiency photon-counting camera and low spectral resolution mode of operation. PAVO disperses spatially-modulated pupil-plane fringes with a resolution $R=40$. The instrument splits the polarization and combines three telescopes, allowing imaging capabilities of relatively faint objects in the visible.

2. The MIRC Combiner

The original idea of using a fibre image-plane combiner at CHARA was introduced by Turner et al. (1994) who wanted to build a six beam visible combiner with single-mode fibres.

The Michigan infrared combiner (MIRC) is an image-plane combiner that uses single-mode fibres and is conceptually similar to Turner et al. (1994) design. MIRC is the only instrument that has presently produced high-resolution images of complex stellar sources at infrared wavelengths. For detailed description of the instrument see Monnier et al. (2004a, 2006, 2008). Figure 3 shows the MIRC table at CHARA. The instrument combines at present four telescopes but is designed to use the full capability of the CHARA array by combining six telescopes.

The highest sensitivity demonstrated at low spectral resolution ($R=40$) has been $m_H=4.5$ and $m_K=3.5$. Fringes were successfully tracked at H band using the $R=150$ grism on Algol and at K band on γ Cas using the $R=400$ grism. The switch to six beams will happen when the CHARA Michigan phase-tracker (CHAMP) is operational (see Section 3). CHAMP will allow

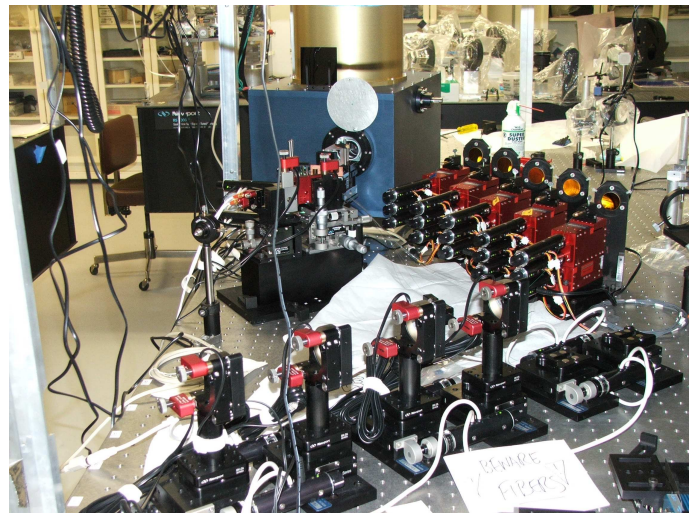


Figure 3: The MIRC combiner at CHARA. The gold-coated off-axis parabolas that focus the incoming telescope beams on the single-mode fibres are visible on the right. At the centre is the PICNIC camera and the focusing optics for the fibered VGroove. Motorised and encoded translation stages are employed everywhere for easy alignment of the optical components of the beam combiner.

coherent fringe integration and consequently access to fainter objects for the CHARA array.

2.1. Optics

MIRC uses single-mode fibres as spatial filters. Light is injected into the fibres using off-axis parabolas. Figure 4 shows a schematic of the MIRC combiner. After spatial filtering the fibres are re-arranged to form a synthetic pupil on a line in a non-redundant pattern, using a commercially available VGroove (top-left of Figure 4). The focusing optics f_p produces an image-plane fringe pattern on the slit of the spectrograph. The focusing optics is not a lens but an off-axis parabola. The fringe pattern is compressed in one dimension by using the cylindrical lens f_c . The compressed pattern is shown on Figure 4 bottom-left. The fringes are then re-collimated using a doublet and dispersed using a non-deviating prism. The prism achieves a spectral resolution of $R=40$.

Alternatively two low-resolution grisms can be used, with a spectral resolution of $R=150$ and $R=450$. Figure 5 shows a more detailed view of the optics after the slit of the spectrograph. The custom-made doublet L_1 is used to re-collimate the image-plane fringes through the dispersive elements. A

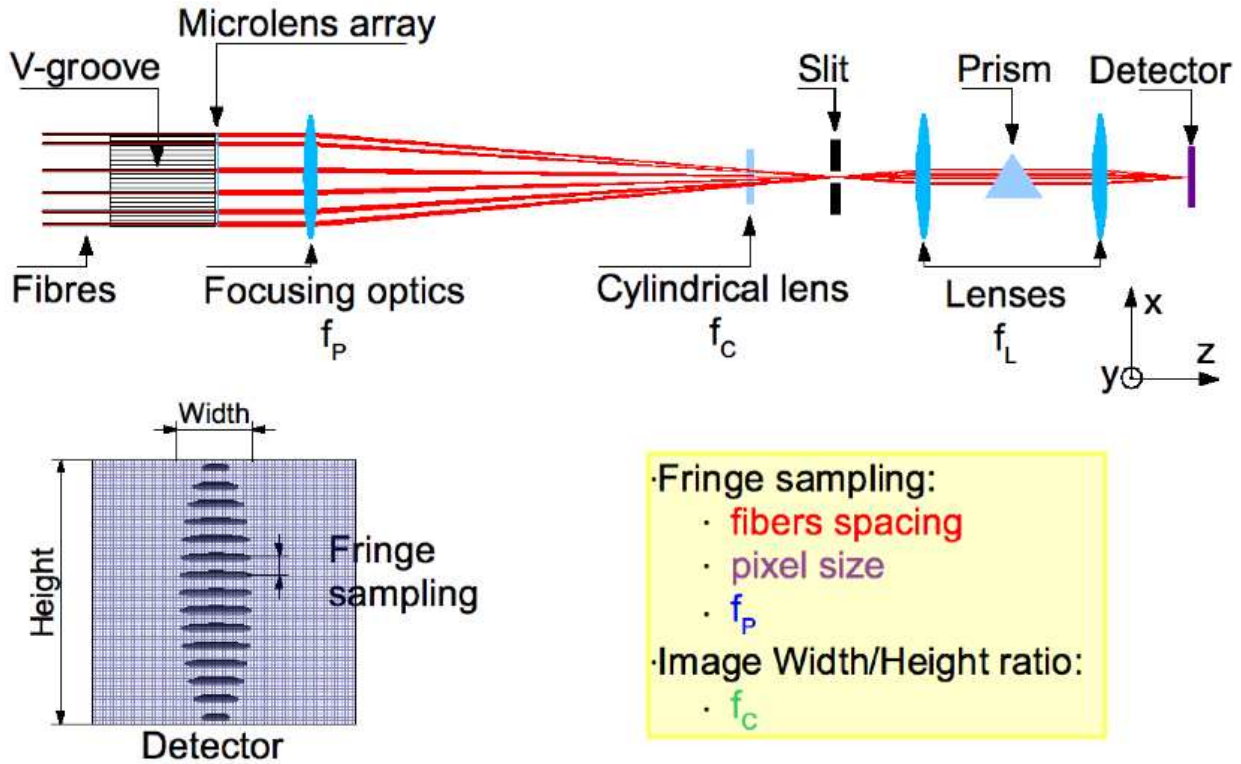


Figure 4: Top: Principle diagram of the MIRC combiner. The fibres from the off-axis parabolas arrive to a VGroove. The beams are collimated by a microlens array and focused on the slit of the spectrograph using the focusing optics f_p and the cylindrical lens f_c . This optical combination compresses the fringes in one direction. The compressed fringe pattern is shown on bottom-left. The one-dimensional fringe pattern is re-collimated by the f_l lens closer to the slit and passes through a non-deviating prism for dispersing the fringes. The fringe pattern is then focused on the PICNIC detector by means of the cryogenic doublet f_l (lens closer to the detector). The fringes have to be re-imaged on the pixels of the detector using at least Nyquist sampling. The chosen sampling was 2.5 fringes per pixel at the shortest wavelength of $1.5\mu\text{m}$. The fringe sampling depends on the spacing of the fibres (determined by the minimum spacing of the fibres in the VGroove), by the size of the pixel ($40\mu\text{m}$) and by the focal length of the focusing optics f_p (bottom-right panel).

filter-wheel can switch among the two gratings or narrow band filters. The custom-made doublet L_2 was designed to work at cryogenic temperatures, its dilatation coefficient modeled to achieve the correct focus at low temperature. Dispersed fringes are imaged on the PICNIC detector shown on the left-hand side of Figure 5. The combiner was built using almost exclusively commercially available components. Designed for imaging, MIRC currently combines four telescopes at once. The wavelength coverage is from 1.5 to $2.4\mu\text{m}$. MIRC is conceptually very similar to the astronomical multi-beam combiner (AMBER) (Petrov et al., 2001; Petrov and The AMBER Consortium, 2003; Weigelt et al., 2005), the imaging combiner for the very large telescope interferometer (VLTI), but was built on a much smaller budget and using less ambitious specifications. The project ran for three years but most of the work was concentrated in the final year before commissioning. Commissioning, from installation to four-telescope fringes and first data, took approximately one month.

In the final six-telescope version MIRC will provide 15 visibilities and 10 independent closure phases. At present, with four telescopes MIRC can only achieve six visibilities and three independent closure-phase triangles. The calibration of the closure phase is intrinsically 0° and the precision is around $0.1^\circ - 0.5^\circ$. Good calibration of the closure phases is much more

important for imaging purpose than the calibration of visibilities, which is rather poor for the MIRC combiner (worse than 10%). An example of the dispersed fringe pattern acquired by the infrared camera is shown in Figure 8.

2.2. Camera electronics and software

The camera developed for the MIRC combiner is based on the PICNIC infrared detector (Kozłowski et al., 2000; Cabelli et al., 2000). The control electronics is the commercially available GEN-RAD2, general-purpose camera controller (Leach et al., 1998) that uses four separate data-acquisition channels which allow parallel readout of the four quadrants of the PICNIC detector. The usual readout mode for the GEN-RAD2 controller was modified from the standard correlated double sampling to fast sub-frame readout and Fowler sampling (Fowler and Gatley, 1991; McLean et al., 1993), which allows non-destructive, fast readout and post-processing integration of the acquired fringe frames. A block diagram of the camera subsystem is shown in Figure 6.

2.2.1. Real-time control software

The real-time control software was discussed in details in Pedretti et al. (2006). Briefly, the GEN-RAD2 controller connects to a server running a modified version of the LINUX operating

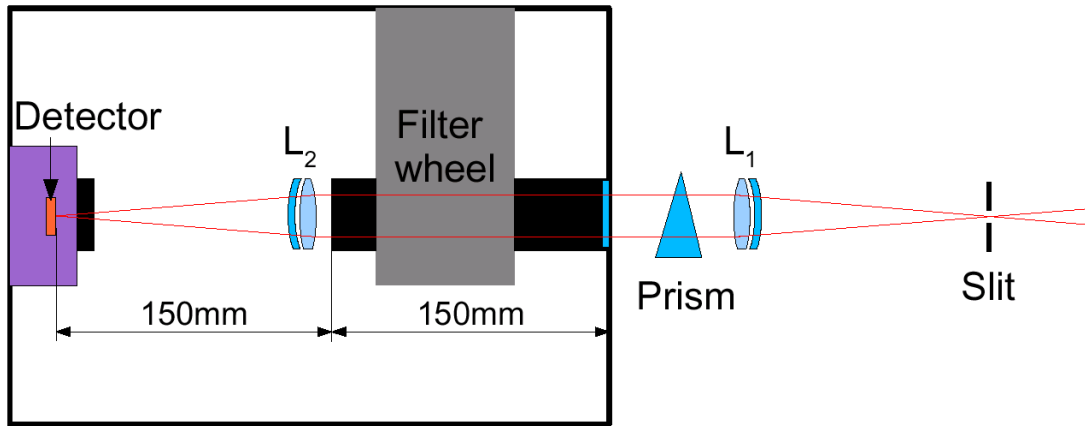


Figure 5: Details of the optics beyond the slit of the spectrograph. The box on the left represents the cryostat of the PICNIC camera. A custom-made doublet (L_2) produces image-plane fringes on the detector. A filter-wheel allows the selection of the bandwidth of operation for the spectrograph, typically H and K band filters. On the right, outside the cryostat there are warm optics. The light from the Vgroove passes through a slit, is collimated by the doublet L_1 and dispersed by the prism. The slit is gold-plated and is supposed to reflect back the cold dewar to the detector and reduce thermal background.

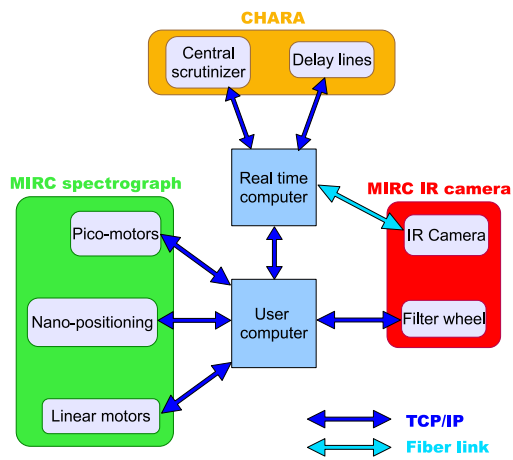


Figure 6: Block diagram of the subsystems composing MIRC including communication with the CHARA array. The real-time computer controls the infrared camera. The main function of the infrared camera is to acquire image-plane interferograms at the maximum readout speed of the infrared detector. The real-time computer stores the interferograms to disc, calculates the optical path error and sends that to the delay lines. The real-time computer also communicates with a “user computer” for data display and user commands.

system that allows real-time operation. Figure 7 shows a block diagram of the software architecture.

The data collected from the infrared camera is deinterlaced. A difference of consecutive frames is performed in order to implement Fowler sampling. Each difference is Fourier transformed for group delay tracking calculation. Data is fed to a non real-time spooler. The spooler is responsible for writing the data to the disc and creating the FITS header by gathering information through a network connection from the various CHARA servers.

2.2.2. Group Delay Tracking

The group delay tracking algorithm was developed at the GI2T interferometer (Koechlin et al., 1996) and controlled the optical path of the single baseline of GI2T. The Fourier transform of the fringe pattern yields a peak for each baseline in the power spectrum. The position of the peaks in Fourier space are related to the optical path error for each baseline. A simple barycentre function yields the position of the peaks. The algorithm was adapted to work with four telescopes using the same method adopted at the IOTA interferometer (Pedretti et al., 2005). The calculated offsets are then sent to the CHARA delay lines through a network connection.

2.2.3. User interface

The graphical user interface (GUI) for the MIRC instrument was discussed in detail in Thureau et al. (2006). Briefly a computer running a standard LINUX distribution is responsible for sending commands to the camera server and displaying information about the current observing session. The interface is also responsible for programming the mode of operation of the camera, searching for fringes, configuring, starting and stopping data acquisition, fringe tracking and shutter sequencing.

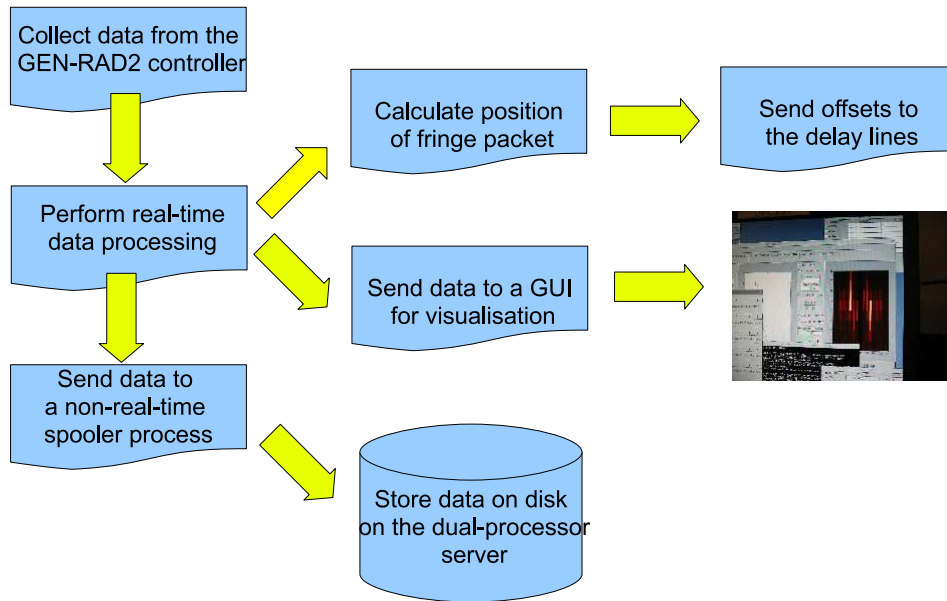


Figure 7: Software functional diagram. The interferograms collected are de-interlaced and Fourier-transformed in order to calculate the optical path error. The offsets are sent to the delay lines through a network connection. When requested by the user computer the interferograms are sent for display through a separate network connection. The data is also sent to a non real-time spooler process that writes data to disc.

2.2.4. Data acquisition sequence

Scripts are run from the user interface in order to perform the observing tasks as a semi-automatic sequence. The observing sequence starts with the CHARA array slewing to a star and acquiring the star in the tip-tilt camera. At the same time the delay lines slew to the model positions. This task is typically completed in five minutes.

The observer then runs a fibre explorer routine which performs a raster-scan of the fibre mount around the focus of the off-axis parabola in order to maximise the coupling of the fibre to the telescope flux. This task takes about ten minutes for four telescopes.

Once the flux is optimised on all telescopes the observer starts searching for fringes. This process is partly automated. The delay lines are automatically moved through a programmed delay range and stop when fringes are found. The observer needs to check that the process runs smoothly. Sometimes the fringes are not detected or they are detected when not present. The detection threshold has to be adjusted empirically depending on the observing conditions. Finding fringes and locking them with the group delay tracker takes about ten minutes for four telescopes.

Once all fringes are locked data can be acquired. Data is usually taken for about five minutes. After data, a shutter sequence is usually taken. Shutter data is acquired: (1) with only one telescope at time, (2) with all the shutters closed (background), (3) with all the shutters opened (foreground) but with fringes not present in the data (this is accomplished by stopping the delay

lines during foreground taking). This sequence typically takes five minutes. Another five minutes of data is usually taken after the shutter matrix. The observing sequence ends with another 5-minutes shutter matrix. The best case cycle is 50 minutes per objects when performing this sequence. Usually calibration data is acquired at the beginning of the night using the same sequence. Three targets can usually be acquired before calibration is again needed.

2.3. Known problems of the MIRC combiner

The use of single-mode fibres and spectral dispersion increases the accuracy of the visibility amplitude measurement provided that the photometric fluctuation caused by the coupling through fibres is monitored. This is achieved by means of “photometric taps”. A photometric tap is a device that extracts a small percentage of the flux from a fibre before beam combination. The MIRC combiner does not currently have photometric taps. Large changes are observed in mean fiber coupling between shutter sets. Choppers have been recently introduced to partially recover the photometric signal but success has been limited: the visibility amplitude accuracy is still somewhat worse than 10%.

The spectral dispersion adopted for MIRC reduces the overall sensitivity of the combiner but is crucial for precision calibration since chromatic effects dominate systematic errors in current single-mode fibres and integrated optic combiners (Monnier et al., 2004b). Other than providing useful informa-

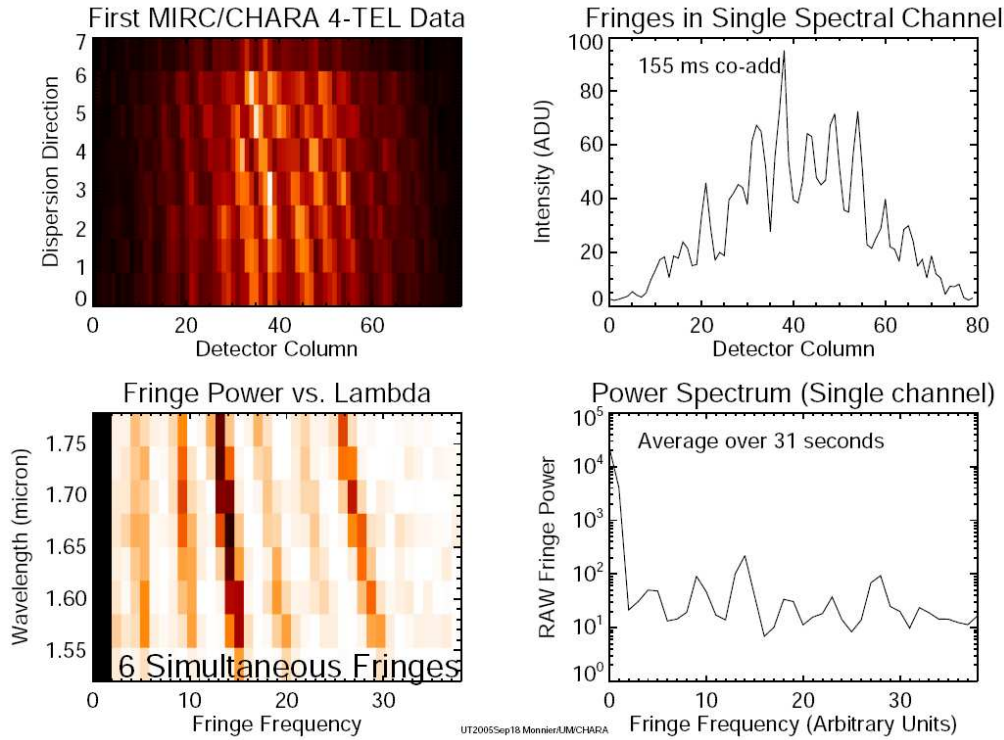


Figure 8: Top-left: dispersed fringe pattern recorded on the PICNIC detector. Top-right: the fringes in a single spectral channel. Bottom-left: the one dimensional power spectrum of every spectral channel showing a change in frequency and therefore in wavelength of the fringe pattern in the vertical direction. Bottom-right: Power spectrum of a single spectral channel.

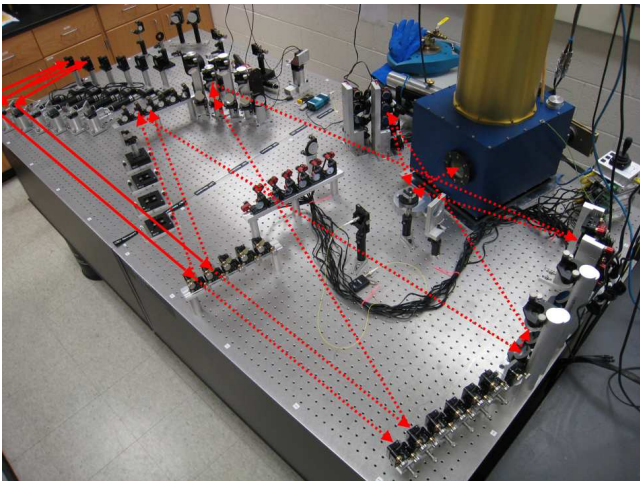


Figure 9: The CHAMP optical table at the University of Michigan. The infrared camera is visible on the left side of the optical table. The optical path for two incoming beams is drawn on the picture.

tion about the target, spectral dispersion is important for imaging since it reduces bandwidth smearing on long baselines.

Combining more than two telescopes at the same time degrades the signal-to-noise ratio of the detected complex visibility: for more than two telescopes the signal for each baseline depends on the combined flux and fringe contrast from the telescope pair, but the noise depends on the photon noise added by

all telescopes. The larger the number of telescopes, the larger the photon noise contribution.

It is also more difficult to find fringes on MIRC if the error on the position of the fringes is larger than one mm. This typically happens at the beginning of an observing run, when the instrument has not been used for a while or when the time server fails on the CHARA computer responsible for the baseline model. At the beginning of a MIRC observing run offsets are typically searched with the CHARA Classic beam combiner for all the baselines in use. We should mention that the baseline solutions and the stability of the time servers is improving at CHARA. We expect the errors in position to be less than a few mm in all configurations soon.

Another practical difficulty of observing with more than two telescopes at time is keeping all delay lines in range. This is much harder with four telescopes, the largest limitation being the E-W baseline. It is also very hard to find bright calibrators because only a limited sky coverage is possible due to the limited delay range.

3. The CHAMP fringe tracker

The CHAMP fringe tracker (Berger et al., 2006b, 2008) is expected to solve some of the problems listed in Section 2.3. CHAMP will be part of the MIRC optical table and will operate on the J/H/K band not used by any science combiner. CHAMP

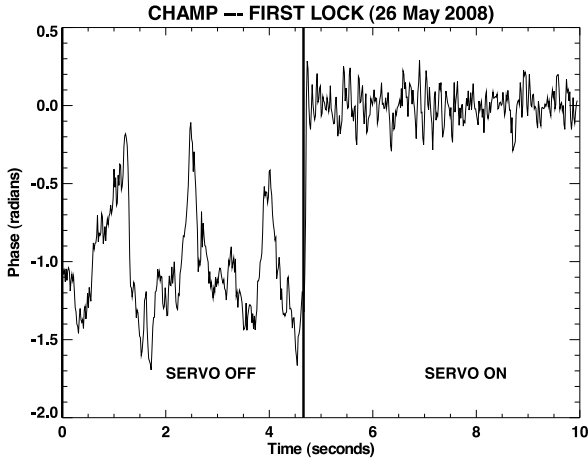


Figure 10: First fringe lock obtained in the laboratory.

was designed for the MIRC combiner but it will be available to all other instruments deployed at CHARA.

This new instrument is expected to improve the magnitude limit of MIRC by three magnitudes by removing the atmospheric piston and virtually freezing the fringes in the time domain. The fringe tracker will allow longer integration time on the science beam combiners, permitting access to fainter objects like young stellar objects and eventually hot Jupiters (van Belle, 2008; Zhao et al., 2008b).

The fringe tracker will phase the array by using a minimum number of telescope pairs. It will also use broad-band, white-light fringes and avoid spatial filtering in order to achieve higher sensitivity. The fringe tracker will measure the fringe phase using the ABCD method (Shao and Colavita, 1992), where a fast dither is applied to the optical path in order to obtain fringes in the temporal domain. The instrument is composed of a bulk-optics beam combiner. The infrared camera is based on the HAWAII-1 array from Rockwell while the optical path is modulated using $8\ \mu\text{m}$ maximum stroke piezo actuators (see Figure 9 for a recent picture of the CHAMP fringe tracker).

4. Data reduction pipeline

The data reduction pipeline is mostly automated and in principle requires minimal user input. An entire night is analysed at once using multiple calibration strategies. The input files in FITS format contain frames of spatially encoded fringes from the beam combiner as explained in Section 2. The data frames are co-added and sub-frames of the area containing fringes extracted. Other areas of the detector that do not contain fringes are used for estimating the noise floor of the detector. Information is then extracted from the FITS header in order to populate the uv plane and add time information to the data. The photometric information from the choppers, shutters and fibre profile is analysed. The wavelength scale is calculated from fringe fitting and by applying a quadratic model to the channels of the spectrometer. The frames are background subtracted and Fourier transformed. Power spectra are accumulated for visibility² estimation after foreground subtraction.

In order to calibrate the photometric fluctuations in the fibres, spinning chopper are used to partially modulate the beams entering the fibres. The beams are modulated at 25,30,35 and 40 Hz so that photometric channels can be extracted in the time domain with a Fourier transform. The temporal loss of coherence caused by the exposure time too long to “freeze” the atmosphere can be calibrated alternating stars of well-known properties and diameters to the science targets. Particular care should be used in choosing the calibrators to avoid binary stars, resolved stars with spots or stars departing from spherical symmetry. The diameter of the calibrator should be carefully chosen since it represents an important source of errors.

Fringe amplitude and phase are combined into a triple product. The closure phase is extracted as the argument of the triple product (Baldwin et al., 1996). The data pipeline was carefully checked against the binary ι Peg (Monnier et al., 2007), a source that was extensively observed at the IOTA interferometer, at the navy prototype optical interferometer (NPOI) and the Palomar testbed interferometer (PTI). The sign of the closure phase was calibrated against ι Peg in order to remove the $+180^\circ$ or -180° ambiguity.

Although the calibration of the closure phase is extremely accurate there are still some issues with the calibration of the visibilities which can be worse than 10% due to lack of photometric channels in the MIRC combiner. The observer is always advised of getting two or three visits of each target, in order to check calibration stability. At the end of the data-reduction process data is saved in full OIFITS data format (Pauls et al., 2005) and summary plots are created for inspecting the data set.

5. Imaging software

The usual approach adopted so far at CHARA is to use model-independent image reconstruction to interpret visibility amplitude and closure-phase data. Two imaging packages are currently used: the Markov-chain imaging software MACIM from Ireland et al. (2006) and bispectrum maximum entropy method (BSMEM) (Buscher, 1994).

The role of image reconstruction is to guide the model. Model-fitting produces the high-precision results as shown in Section 6. There is not a specific package used for model fitting. So far investigators developed their own software in order to produce models of the OIFITS data.

6. Results

We will present a selection of the imaging results obtained in the last three years at the CHARA array. The images were obtained using the MACIM and CLEAN (Högbom, 1974) imaging package. We also show models which were used to obtain the physical parameters of the objects.

6.1. Rapid rotators

In hot stars the absence of magnetic fields is expected to prevent the star from spinning down after formation. The effect of rapid rotation is two-fold: (1) it distorts the stellar photosphere,

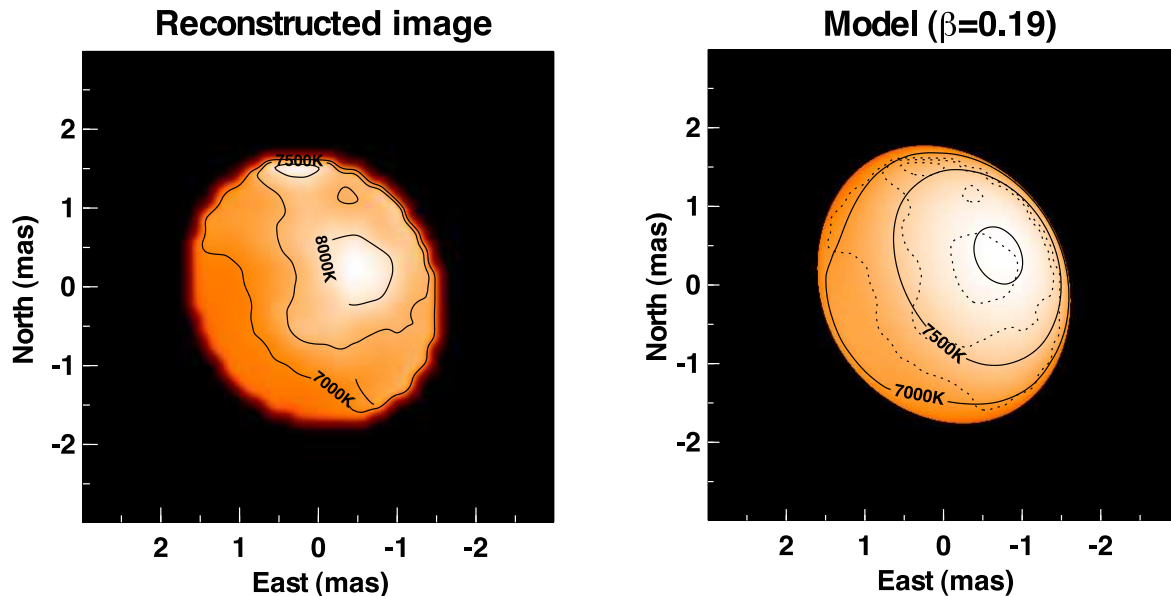


Figure 11: The first image of a main sequence star other than the Sun (Monnier et al., 2007). Altair is a nearby rapidly rotating star. The left panel shows a model-independent image reconstruction obtained by MACIM from visibility and closure phase obtained by the MIRC combiner at the CHARA array. Gravity darkening is evident in this image. The right panel shows a model-dependent image reconstruction based on the von Zeipel (1924a,b) model.

rendering the radius larger at the equator than at the pole (2) it produces “gravity darkening” at the equator due to the reduced surface gravity and effective temperature caused by increased equatorial radius.

Rapid rotation can also change interior angular momentum and cause differential rotation. Abundance anomalies have been reported due to rotation-induced mixing (Pinsonneault, 1997). Some investigators also report that rapid rotation can alter the H-R diagram mass-luminosity relation (Maeder and Meynet, 2000a,b).

Monnier et al. (2007) obtained the first image of a rapidly-rotating main-sequence star at CHARA using the MIRC combiner. Altair is a nearby (5.1 pc) hot star (A7V, $T=7850$ K) that is rotating at about 90% breakup speed ($v \sin i = 240$ km/s).

Figure 11 shows a model-independent image of Altair compared against the basic model of von Zeipel (1924a,b). Units are in milliarcseconds (mas). These results were based on model-fitting of interferometry data with a few baselines. The model assumes solid body rotation, a Roche potential (central point mass) and simplistic radiative transfer model for the outer layers (Aufdenberg et al., 2006). The resemblance of the image to the prediction of the model is quite obvious but there are some discrepancies.

When a gravity-darkening coefficient $\beta=0.25$ is used for the von Zeipel model of a fast-rotating star with a radiative envelope, the model is a poor fit of the measured visibilities. The equator is cooler than what is expected from the von Zeipel law. When β is left a free parameter the temperature profiles are more consistent with $\beta=0.19$. Hydro-dynamical models suggest possible solutions in non-solid body rotation, for example, differential rotation and meridional flows (Jackson et al., 2004; MacGregor et al., 2007; Espinosa Lara and Rieutord, 2007).

6.2. Binary stars

Binary stars were often studied with optical interferometry being relatively simple objects to model or image. Often the components are very close and can only be resolved by the long baseline of an interferometer. The first model-independent image from long-baseline optical interferometry was the binary star Capella (Baldwin et al., 1996). Interferometric observations can measure the apparent size, orientation and inclination of the orbit. The inclination combined with the spectroscopic orbit yields the masses of the components.

Second-generation interferometers like CHARA and the VLTI, which have long baselines and several apertures are able to image the circumstellar environment of close binary systems. Interacting binaries are great laboratories for testing the tidal interaction of the components, mass transfer and accretion processes. They are interesting to study the evolution of the components, often progenitor of X-ray binaries, where one of the objects eventually evolves into a neutron star or a black hole. Although interacting binaries have been studied with spectroscopy and photometry they are very challenging for imaging due to their great distance and small apparent separation.

β Lyrae is an interacting and eclipsing binary with a period of 12.9 days with a B6-8 II spectral-type donor and early B spectral-type gainer surrounded by a thick accretion disc (Harmanec, 2002). It is also the tightest binary system ever resolved by any telescope. The β Lyrae system is very bright ($m_v = 3.52$ and $m_i = 3.35$) with a distance of 296 ± 16 pc (van Leeuwen, 2007). Data was obtained with the MIRC combiner at CHARA and analysed by Zhao et al. (2008a) Figure 12 shows a sequence of six images corresponding to six orbital phases of the binary obtained with three independent methods: the MACIM imaging package, BSMEM and a simple, two-component, binary

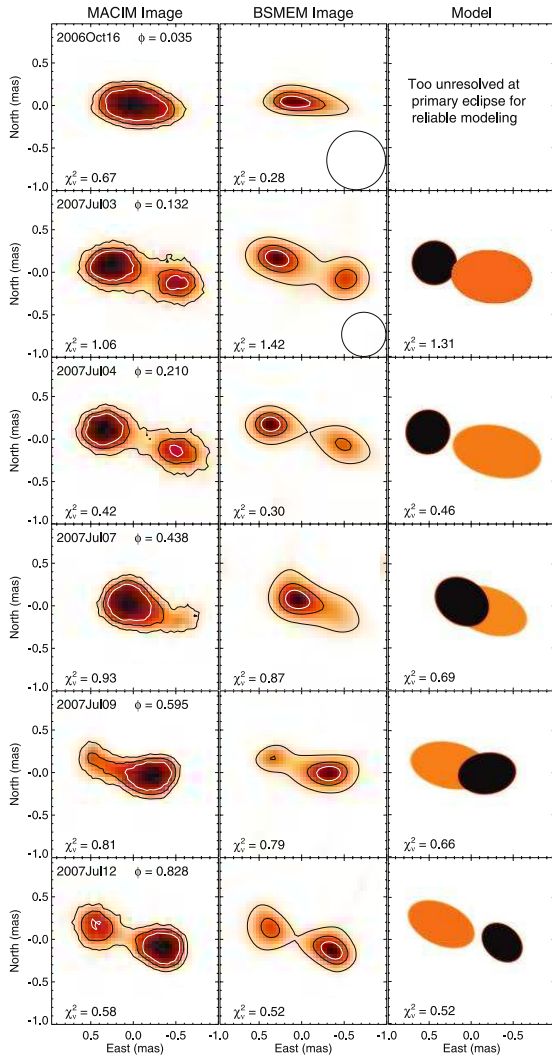


Figure 12: Snapshots images of the binary star β Lyrae across different phases of the orbital period (Zhao et al., 2008a). Images obtained through MACIM and BSMEM are shown in the first and second column from the left. The images partially resolves the accretion disc between the two stars. A simple two-component model of the binary system is shown on the right column.

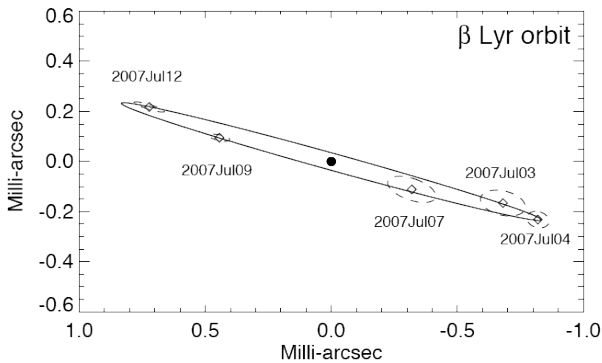


Figure 13: The astrometric orbit of β Lyrae (Zhao et al., 2008a).

model. Astrometric positions obtained from the images and from the model were sufficient to determine the astrometric orbit of β Lyrae shown on Figure 13

Orbital parameters and distance to the system were also derived and can be found in Zhao et al. (2008a). Precise mass for the gainer of $12.76 \pm 0.27 M_{\odot}$ and for the donor of $2.83 \pm 0.18 M_{\odot}$ could be estimated.

7. Summary

In its first three years of operation MIRC obtained the first images of main sequence stars besides the Sun. MIRC confirmed that distortion and gravity darkening are observed in rapid rotators and suggested that temperatures profiles are not consistent with von Zeipel law, suggesting differential rotation as a possible cause of the discrepancy.

High angular resolution images of interacting binaries are now possible. The physics of accretion discs in close binaries can now be studied with long-baseline infrared interferometry. Studies of magnetic fields and star spots in active stars is underway, combining interferometry and Doppler imaging techniques.

The imaging of the discs of young stellar object will be achieved at the CHARA array when the CHAMP fringe tracker is operational, allowing access to fainter targets.

References

- Aufdenberg, J. P., Mérand, A., Coudé du Foresto, V., Absil, O., Di Folco, E., Kervella, P., Ridgway, S. T., Berger, D. H., ten Brummelaar, T. A., McAlister, H. A., Sturmman, J., Sturmman, L., Turner, N. H., Jul. 2006. First Results from the CHARA Array. VII. Long-Baseline Interferometric Measurements of Vega Consistent with a Pole-On, Rapidly Rotating Star. *ApJ*645, 664–675.
- Bagnuolo, Jr., W. G., Taylor, S. F., McAlister, H. A., ten Brummelaar, T., Gies, D. R., Ridgway, S. T., Sturmman, J., Sturmman, L., Turner, N. H., Berger, D. H., Gudehus, D., May 2006. First Results from the CHARA Array. V. Binary Star Astrometry: The Case of 12 Persei. *AJ*131, 2695–2699.
- Baines, E. K., van Belle, G. T., ten Brummelaar, T. A., McAlister, H. A., Swain, M., Turner, N. H., Sturmman, L., Sturmman, J., Jun. 2007. Direct Measurement of the Radius and Density of the Transiting Exoplanet HD 189733b with the CHARA Array. *ApJ*661, L195–L198.
- Baldwin, J. E., Beckett, M. G., Boysen, R. C., Burns, D., Buscher, D. F., Cox, G. C., Haniff, C. A., Mackay, C. D., Nightingale, N. S., Rogers, J., Scheuer, P. A. G., Scott, T. R., Tuthill, P. G., Warner, P. J., Wilson, D. M. A., Wilson, R. W., Feb. 1996. The first images from an optical aperture synthesis array: mapping of Capella with COAST at two epochs. *A&A*306, L13+.
- Berger, D. H., Gies, D. R., McAlister, H. A., ten Brummelaar, T. A., Henry, T. J., Sturmman, J., Sturmman, L., Turner, N. H., Ridgway, S. T., Aufdenberg, J. P., Mérand, A., Jun. 2006a. First Results from the CHARA Array. IV. The Interferometric Radii of Low-Mass Stars. *ApJ*644, 475–483.
- Berger, D. H., Monnier, J. D., Millan-Gabet, R., ten Brummelaar, T. A., Anderson, M., Blum, J. L., Blasius, T., Pedretti, E., Thureau, N., Jul. 2008. CHARA Michigan phase-tracker (CHAMP): a preliminary performance report. In: Society of Photo-Optical Instrumentation Engineers (SPIE) Conference Series. Vol. 7013 of Presented at the Society of Photo-Optical Instrumentation Engineers (SPIE) Conference.
- Berger, D. H., Monnier, J. D., Millan-Gabet, R., ten Brummelaar, T. A., Muirhead, P., Pedretti, E., Thureau, N., Jul. 2006b. CHARA Michigan phase-tracker (CHAMP): design and fabrication. In: Society of Photo-Optical Instrumentation Engineers (SPIE) Conference Series. Vol. 6268 of Presented at the Society of Photo-Optical Instrumentation Engineers (SPIE) Conference.

- Blazit, A., Rondeau, X., Thiébaud, É., Abe, L., Bernengo, J.-C., Chevassut, J.-L., Clausse, J.-M., Dubois, J.-P., Foy, R., Mourard, D., Patru, F., Spang, A., Tallon-Bosc, I., Tallon, M., Tourneur, Y., Vakili, F., Mar. 2008. New generation photon-counting cameras: algol and CPNG. *Appl. Opt.* 47, 1141–1151.
- Buscher, D. F., 1988. Ph.D. Thesis.
URL http://adsabs.harvard.edu/cgi-bin/nph-bib_query?bibcode=1988PhDT.....202B&db_key=AST
- Buscher, D. F., 1994. Direct maximum-entropy image reconstruction from the bispectrum. In: Robertson, J. G., Tango, W. J. (Eds.), *Very High Angular Resolution Imaging*. Vol. 158 of IAU Symposium. pp. 91–+.
- Cabelli, C. A., Cooper, D. E., Haas, A. K., Kozłowski, L. J., Bostrup, G. L., Chen, A. C., Blackwell, J. D., Montroy, J. T., Vural, K., Kleinhans, W. E., Hodapp, K., Hall, D. N., Jul. 2000. Latest results on HgCdTe 2048x2048 and silicon focal plane arrays. In: *Proc. SPIE, Infrared Detectors and Focal Plane Arrays VI*, Eustace L. Dereniak; Robert E. Sampson; Eds. Vol. 4028. pp. 331–342.
- Chesneau, O., Rousset-Perraut, K., Vakili, F., Mourard, D., Cazale, C., Jul. 2000. Polarimetric interferometry: concept and applications. In: Léna, P., Quirrenbach, A. (Eds.), *Society of Photo-Optical Instrumentation Engineers (SPIE) Conference Series*. Vol. 4006 of Presented at the Society of Photo-Optical Instrumentation Engineers (SPIE) Conference. pp. 531–540.
- Coudé du Foresto, V., Borde, P. J., Merand, A., Baudouin, C., Remond, A., Perrin, G. S., Ridgway, S. T., ten Brummelaar, T. A., McAlister, H. A., Feb. 2003. FLUOR fibered beam combiner at the CHARA array. In: Traub, W. A. (Ed.), *Society of Photo-Optical Instrumentation Engineers (SPIE) Conference Series*. Vol. 4838 of Society of Photo-Optical Instrumentation Engineers (SPIE) Conference Series. pp. 280–285.
- Coudé du Foresto, V., Perrin, G., Mariotti, J.-M., Lacasse, M., Traub, W., 1997. The FLUOR/IOTA fiber stellar interferometer. *Integrated Optics for Astronomical Interferometry*, pp. 115–125.
- Coudé du Foresto, V., Ridgway, S. T., Mar. 1992. Fluor - a Stellar Interferometer Using Single-Mode Fibers. In: Beckers, J. M., Merkle, F. (Eds.), *European Southern Observatory Astrophysics Symposia*. Vol. 39 of European Southern Observatory Astrophysics Symposia. pp. 731–+.
- Dyck, H. M., Benson, J. A., Carleton, N. P., Coldwell, C., Lacasse, M. G., Nisenson, P., Panasyuk, A., Pappalios, C., Pearlman, M. R., Reasenberg, R. D., Traub, W. A., Xu, A., Predmore, C. R., Schloerb, F. P., Gibson, D. M., Jan. 1995. First 2.2 micrometer results from the IOTA interferometer. *AJ* 109, 378–382.
- Espinosa Lara, F., Rieutord, M., Aug. 2007. The dynamics of a fully radiative rapidly rotating star enclosed within a spherical box. *A&A* 470, 1013–1022.
- Fowler, A. M., Gatley, I., Nov. 1991. Noise reduction strategy for hybrid IR focal-plane arrays. In: *Proc. SPIE Vol. 1541*, p. 127–133, *Infrared Sensors: Detectors, Electronics, and Signal Processing*, T. S. Jayadev; Ed. pp. 127–133.
- Harmanec, P., Jul. 2002. The ever challenging emission-line binary beta Lyrae. *Astronomische Nachrichten* 323, 87–98.
- Högbom, J. A., Jun. 1974. Aperture Synthesis with a Non-Regular Distribution of Interferometer Baselines. *A&AS* 15, 417–+.
- Ireland, M. J., Mérand, A., ten Brummelaar, T. A., Tuthill, P. G., Schaefer, G. H., Turner, N. H., Sturmman, J., Sturmman, L., McAlister, H. A., Jul. 2008. Sensitive visible interferometry with PAVO. In: *Society of Photo-Optical Instrumentation Engineers (SPIE) Conference Series*. Vol. 7013 of Society of Photo-Optical Instrumentation Engineers (SPIE) Conference Series.
- Ireland, M. J., Monnier, J. D., Thureau, N., Jul. 2006. Monte-Carlo imaging for optical interferometry. In: *Society of Photo-Optical Instrumentation Engineers (SPIE) Conference Series*. Vol. 6268 of Presented at the Society of Photo-Optical Instrumentation Engineers (SPIE) Conference.
- Jackson, S., MacGregor, K. B., Skumanich, A., May 2004. Models for the Rapidly Rotating Be Star Achernar. *ApJ* 606, 1196–1199.
- Jennison, R. C., 1958. A phase sensitive interferometer technique for the measurement of the Fourier transforms of spatial brightness distributions of small angular extent. *MNRAS* 118, 276–+.
- Koechlin, L., Lawson, P. R., Mourard, D., Blazit, A., Bonneau, D., Morand, F., Stee, P., Tallon-Bosc, I., Vakili, F., Jun. 1996. Dispersed fringe tracking with the multi- r_0 apertures of the Grand Interferometre a 2 Telescopes. *Appl. Opt.* 35, 3002–3009.
URL http://adsabs.harvard.edu/cgi-bin/nph-bib_query?bibcode=1996ApOpt...35.3002K&db_key=INST
- Kozłowski, L. J., Montroy, J. T., Cabelli, C. A., Cooper, D. E., Chen, A. C., Bostrup, G. L., Bai, Y., Vural, K., Hodapp, K., Hall, D. N., Aug. 2000. Visible and infrared detectors at Rockwell Science Center. In: *Proc. SPIE, Optical and IR Telescope Instrumentation and Detectors*, Masanori Iye; Alan F. Moorwood; Eds. Vol. 4008. pp. 1240–1253.
- Labeyle, A., Mar. 1975. Interference fringes obtained on VEGA with two optical telescopes. *ApJ* 196, L71–L75.
- Labeyle, A., Schumacher, G., Dugue, M., Thom, C., Bourlon, P., Jul. 1986. Fringes obtained with the large 'boules' interferometer at CERGA. *A&A* 162, 359–364.
- Leach, R. W., Beale, F. L., Eriksen, J. E., Jul. 1998. New-generation CCD controller requirements and an example: the San Diego State University generation II controller. In: D'Odorico, S. (Ed.), *Proc. SPIE Vol. 3355*, p. 512–519, *Optical Astronomical Instrumentation*, Sandro D'Odorico; Ed. pp. 512–519.
- MacGregor, K. B., Jackson, S., Skumanich, A., Metcalfe, T. S., Jul. 2007. On the Structure and Properties of Differentially Rotating, Main-Sequence Stars in the 1–2 M_{Solar} Range. *ApJ* 663, 560–572.
- Maeder, A., Meynet, G., Sep. 2000a. Stellar evolution with rotation. VI. The Eddington and Omega -limits, the rotational mass loss for OB and LBV stars. *A&A* 361, 159–166.
- Maeder, A., Meynet, G., 2000b. The Evolution of Rotating Stars. *ARA&A* 38, 143–190.
- McAlister, H. A., ten Brummelaar, T. A., Gies, D. R., Huang, W., Bagnuolo, Jr., W. G., Shure, M. A., Sturmman, J., Sturmman, L., Turner, N. H., Taylor, S. F., Berger, D. H., Baines, E. K., Grundstrom, E., Ogden, C., Ridgway, S. T., van Belle, G., Jul. 2005. First Results from the CHARA Array. I. An Interferometric and Spectroscopic Study of the Fast Rotator α Leonis (Regulus). *ApJ* 628, 439–452.
- McLean, I. S., Becklin, E. E., Brims, G., Canfield, J., Casement, L. S., Figer, D. F., Henriquez, F., Huang, A., Liu, T., Macintosh, B. A., Teplitz, H., Oct. 1993. UCLA double-beam infrared camera system. In: *Proc. SPIE Vol. 1946*, p. 513–533, *Infrared Detectors and Instrumentation*, Albert M. Fowler; Ed. pp. 513–533.
- Mérand, A., Kervella, P., Coudé Du Foresto, V., Ridgway, S. T., Aufdenberg, J. P., Ten Brummelaar, T. A., Berger, D. H., Sturmman, J., Sturmman, L., Turner, N. H., McAlister, H. A., Jul. 2005. The projection factor of δ Cephei. A calibration of the Baade-Wesselink method using the CHARA Array. *A&A* 438, L9–L12.
- Monnier, J. D., Oct. 2007. Phases in interferometry. *New Astronomy Review* 51, 604–616.
- Monnier, J. D., Berger, J.-P., Millan-Gabet, R., Ten Brummelaar, T. A., Oct. 2004a. The Michigan Infrared Combiner (MIRC): IR imaging with the CHARA Array. In: Traub, W. A. (Ed.), *Society of Photo-Optical Instrumentation Engineers (SPIE) Conference Series*. Vol. 5491 of Presented at the Society of Photo-Optical Instrumentation Engineers (SPIE) Conference. pp. 1370–+.
- Monnier, J. D., Pedretti, E., Thureau, N., Berger, J.-P., Millan-Gabet, R., ten Brummelaar, T., McAlister, H., Sturmman, J., Sturmman, L., Muirhead, P., Tannirkulam, A., Webster, S., Zhao, M., Jul. 2006. Michigan Infrared Combiner (MIRC): commissioning results at the CHARA Array. In: *Society of Photo-Optical Instrumentation Engineers (SPIE) Conference Series*. Vol. 6268 of Presented at the Society of Photo-Optical Instrumentation Engineers (SPIE) Conference.
- Monnier, J. D., Traub, W. A., Schloerb, F. P., Millan-Gabet, R., Berger, J.-P., Pedretti, E., Carleton, N. P., Kraus, S., Lacasse, M. G., Brewer, M., Ragland, S., Ahearn, A., Coldwell, C., Feb. 2004b. First Results with the IOTA3 Imaging Interferometer: The Spectroscopic Binaries λ Virginis and WR 140. *ApJ* 602, L57–L60.
- Monnier, J. D., Zhao, M., Pedretti, E., Thureau, N., Ireland, M., Muirhead, P., Berger, J.-P., Millan-Gabet, R., Van Belle, G., ten Brummelaar, T., McAlister, H., Ridgway, S., Turner, N., Sturmman, L., Sturmman, J., Berger, D., Jul. 2007. Imaging the Surface of Altair. *Science* 317, 342–.
- Monnier, J. D., Zhao, M., Pedretti, E., Thureau, N., Ireland, M., Muirhead, P., Berger, J.-P., Millan-Gabet, R., Van Belle, G., ten Brummelaar, T., McAlister, H., Ridgway, S., Turner, N., Sturmman, L., Sturmman, J., Berger, D., Tannirkulam, A., Blum, J., Jul. 2008. Imaging the surface of Altair and a MIRC update. In: *Society of Photo-Optical Instrumentation Engineers (SPIE) Conference Series*. Vol. 7013 of Presented at the Society of Photo-Optical Instrumentation Engineers (SPIE) Conference.
- Mourard, D., Blazit, A., Bonneau, D., Merlin, D., Tallon-Bosc, I., Vakili, F.,

- Menardi, S., Rebattu, S., Hill, L., Rousselet, K., Boit, J.-L., Le Merrer, J., Lasselien-Waultier, G., Saisse, M., Pouliquen, D., Joubert, M., Jun. 1994. REGAIN: a new optical beam combiner for the G12T. In: Breckinridge, J. B. (Ed.), Society of Photo-Optical Instrumentation Engineers (SPIE) Conference Series. Vol. 2200 of Society of Photo-Optical Instrumentation Engineers (SPIE) Conference Series. pp. 593–598.
- Mourard, D., Perraut, K., Bonneau, D., Clause, J. M., Stee, P., Tallon-Bosc, I., Kervella, P., Hughes, Y., Marcotto, A., Blazit, A., Chesneau, O., Domiciano de Souza, A., Foy, R., Hénault, F., Mattei, D., Merlin, G., Roussel, A., Tallon, M., Thiebaut, E., McAlister, H., ten Brummelaar, T., Sturmman, J., Sturmman, L., Turner, N., Farrington, C., Goldfinger, P. J., Jul. 2008. VEGA: a new visible spectrograph and polarimeter on the CHARA Array. In: Society of Photo-Optical Instrumentation Engineers (SPIE) Conference Series. Vol. 7013 of Society of Photo-Optical Instrumentation Engineers (SPIE) Conference Series.
- Pauls, T. A., Young, J. S., Cotton, W. D., Monnier, J. D., Nov. 2005. A Data Exchange Standard for Optical (Visible/IR) Interferometry. PASP117, 1255–1262.
- Pedretti, E., Monnier, J. D., Thureau, N. D., Berger, D. H., Jul. 2006. A freely available real-time operating system well suited for astronomy and the physical sciences. In: Society of Photo-Optical Instrumentation Engineers (SPIE) Conference Series. Vol. 6268 of Presented at the Society of Photo-Optical Instrumentation Engineers (SPIE) Conference.
- Pedretti, E., Traub, W. A., Monnier, J. D., Millan-Gabet, R., Carleton, N. P., Schloerb, F. P., Brewer, M. K., Berger, J.-P., Lacasse, M. G., Ragland, S., Sep. 2005. Robust determination of optical path difference: fringe tracking at the Infrared Optical Telescope Array interferometer. Appl. Opt.44, 5173–5179.
- Petrov, R. G., Malbet, F., Richichi, A., Hofmann, K.-H., Mourard, D., The Amber Consortium, 2001. AMBER : a near infrared focal instrument for the VLTI. Comptes Rendus Physique 2, 67–97.
- Petrov, R. G., The AMBER Consortium, 2003. Introducing the near infrared VLTI instrument AMBER to its users. Ap&SS286, 57–67.
- Pinsonneault, M., 1997. Mixing in Stars. ARA&A35, 557–605.
- Shao, M., Colavita, M. M., 1992. Long-baseline optical and infrared stellar interferometry. ARA&A30, 457–498.
- Shao, M., Colavita, M. M., Hines, B. E., Staelin, D. H., Hutter, D. J., Mar. 1988. The Mark III stellar interferometer. A&A193, 357–371.
- ten Brummelaar, T. A., McAlister, H. A., Ridgway, S. T., Bagnuolo, Jr., W. G., Turner, N. H., Sturmman, L., Sturmman, J., Berger, D. H., Ogden, C. E., Cadman, R., Hartkopf, W. I., Hopper, C. H., Shure, M. A., Jul. 2005. First Results from the CHARA Array. II. A Description of the Instrument. ApJ628, 453–465.
- Thureau, N. D., Ireland, M., Monnier, J. D., Pedretti, E., Jul. 2006. Software tools for optical interferometry. In: Society of Photo-Optical Instrumentation Engineers (SPIE) Conference Series. Vol. 6268 of Presented at the Society of Photo-Optical Instrumentation Engineers (SPIE) Conference.
- Turner, N. H., ten Brummelaar, T. A., McAlister, H. A., May 1994. A Prototype Visible Imager for the CHARA Array. In: Bulletin of the American Astronomical Society. Vol. 26 of Bulletin of the American Astronomical Society. pp. 895–+.
- van Belle, G. T., May 2008. Closure Phase Signatures of Planet Transit Events. PASP120, 617–624.
- van Belle, G. T., Ciardi, D. R., ten Brummelaar, T., McAlister, H. A., Ridgway, S. T., Berger, D. H., Goldfinger, P. J., Sturmman, J., Sturmman, L., Turner, N., Boden, A. F., Thompson, R. R., Coyne, J., Jan. 2006. First Results from the CHARA Array. III. Oblateness, Rotational Velocity, and Gravity Darkening of Alderamin. ApJ637, 494–505.
- van Leeuwen, F. (Ed.), 2007. Hipparcos, the New Reduction of the Raw Data. Vol. 250 of Astrophysics and Space Science Library.
- von Zeipel, H., Jun. 1924a. The radiative equilibrium of a rotating system of gaseous masses. MNRAS84, 665–683.
- von Zeipel, H., Jun. 1924b. The radiative equilibrium of a slightly oblate rotating star. MNRAS84, 684–701.
- Weigelt, G., Beckert, T., Beckmann, U., Driebe, T., Foy, R., Fraix-Burnet, D., Hofmann, K.-H., Kraus, S., Malbet, F., Mathias, P., Marconi, A., Monin, J.-L., Petrov, R., Schertl, D., Stee, P., Testi, L., Aug. 2005. Near-infrared Interferometry with the AMBER Instrument of the VLTI. Astronomische Nachrichten 326, 572–572.
- Zhao, M., Gies, D., Monnier, J. D., Thureau, N., Pedretti, E., Baron, F., Merand, A., ten Brummelaar, T., McAlister, H., Ridgway, S. T., Turner, N., Sturmman, J., Sturmman, L., Farrington, C., Goldfinger, P. J., Sep. 2008a. First Resolved Images of the Eclipsing and Interacting Binary β Lyrae. ApJ684, L95–L98.
- Zhao, M., Monnier, J. D., ten Brummelaar, T., Pedretti, E., Thureau, N. D., Jul. 2008b. Exoplanet studies with CHARA-MIRC. In: Society of Photo-Optical Instrumentation Engineers (SPIE) Conference Series. Vol. 7013 of Society of Photo-Optical Instrumentation Engineers (SPIE) Conference Series.